Springer

Acta Mechanica Sinica

CrossMark click for updates

• RESEARCH PAPER •

Acta Mech. Sin., Vol. 39, 122193 (2023)
https://doi.org/10.1007/s10409-022-22193-x

On the accuracy of two-temperature models for hypersonic nonequilibrium flow

Xiaoyong Wang[1], Qizhen Hong[1,2], Yuan Hu[1*], and Quanhua Sun[1,2*]

[1] *State Key Laboratory of High Temperature Gas Dynamics, Institute of Mechanics, Chinese Academy of Sciences, Beijing 100190, China;*
[2] *School of Engineering Science, University of Chinese Academy of Sciences, Beijing 100049, China*

Received May 30, 2022; accepted July 27, 2022; published online September 21, 2022

Due to the empirical assumptions, the widely-used two-temperature models for hypersonic nonequilibrium flow include considerable uncertainties. To overcome the limitations and shortcomings of two-temperature models, the modified Macheret-Fridman model is developed based on the correction method of the modified Marrone-Treanor model. Some typical test cases are employed to assess the accuracy of the modified and widely-used two-temperature models. Furthermore, the reason for improving the accuracy of modified two-temperature models is analyzed and discussed. This work indicates that the correction method based on the modified Marrone-Treanor model is easily applied and extended to the other widely-used two-temperature models, significantly improving their accuracy. In addition, modeling highly nonequilibrium dissociating flows requires considering three critical respects, i.e., the dissociation rates, the vibration-dissociation coupling effect, and the non-Boltzmann effect. The non-Boltzmann effect reduces the dissociation rates and vibrational energy per dissociation. Comparatively, the dissociation rates have more influence than changing the value of the non-Boltzmann factor for vibrational energy loss per dissociation. Future work can focus on enhancing the accuracy of the dissociation rates to improve the accuracy of widely-used two-temperature models.

Nonequilibrium flow, Two-temperature model, Quasi-classical trajectory, Non-Boltzmann effect, Vibration-dissociation coupling effect

Citation: X. Wang, Q. Hong, Y. Hu, and Q. Sun, On the accuracy of two-temperature models for hypersonic nonequilibrium flow, Acta Mech. Sin. **39**, 122193 (2023), https://doi.org/10.1007/s10409-022-22193-x

1. Introduction

In recent years, the interest in the development of hypersonic vehicles has been significantly increasing [1,2]. As a vehicle cruising at hypersonic speeds, a strong bow shock wave envelops the vehicle, and much of kinetic energy is converted to internal energy, resulting in an extremely high temperature in the shock layer [3,4]. The elevated temperatures in hypersonic flows give rise to many complicated physical and chemical processes, such as vibrational and electronic energy excitation, dissociation of molecules, and even ionization [2-6]. As the rates of internal energy excitation and chemical reactions are often comparable to the time scales of flow, the hypersonic flow is always in a state of nonequilibrium [2-4]. Accurately modeling the nonequilibrium flows is very important for the design and development of hypersonic vehicles [3].

A key aspect of chemical nonequilibrium is its two-way coupling to thermal nonequilibrium [7], which has been a research emphasis for a long time. For instance, the thermal nonequilibrium is essential for the chemical kinetics because the dissociation occurs more efficiently when the molecules contain substantial energy in the internal, primarily vibrational modes [7, 8]. In turn, in the course of molecule formation and destruction, the dissociation promotes thermal nonequilibrium [8, 9]. It is well known that the dissociation removes more energy from the vibrational mode than other modes, resulting in nonequilibrium among different internal energies [7-9]. Recent studies have further revealed

*Corresponding authors. E-mail addresses: yhu@imech.ac.cn (Yuan Hu); qsun@imech.ac.cn (Quanhua Sun)
Executive Editor: Xueming Shao

that nonequilibrium exists within each internal energy [7-9]. As a result of easier dissociation of molecules in higher vibrational states, the vibrational energy distributions will strongly deviate from the Boltzmann right behind the bow shock and near the wall surface [9].

Nowadays, two different methods have been proposed to describe the aforementioned chemical-thermal coupling effect: the multi-temperature and state-to-state (StS) model [9]. The two-temperature model is widely used and has been implemented in well-known computational fluid dynamics (CFD) codes [10-12]. In the two-temperature model, each internal energy is assumed to follow a Boltzmann distribution corresponding to its equilibrium temperature [9, 11, 13]. Therefore, its applicability is limited to the flow where vibrational distribution slightly deviates from equilibrium. Furthermore, the reaction rate coefficients utilized in the two-temperature model are based primarily on the decades-old shock-tube data [7, 13]. Due to the measurement and systematic error induced by neglecting the effects of thermal nonequilibrium, a significant amount of uncertainties still exist in the chemical kinetic rates [7]. Based on the recent advances in computational chemistry, the StS model has been developed to overcome the deficiencies of the two-temperature model [7, 9, 14-18]. The StS model treats each internal energy state as a pseudo-species and tracks the population of the states directly [9, 17, 18]. Consequently, the non-Boltzmann distribution of internal energy can be resolved [9, 17, 18]. However, the StS model requires numerous rate coefficients for all the excitation and dissociation processes of every internal energy state [9, 18]. On the whole, due to hundreds of internal energy states and thousands or tens of thousands of kinetic processes to be considered, CFD with the StS model is exceptionally computationally demanding. As a result, its application is mainly restricted to simplified zero- or one-dimensional cases so far [9, 14, 19, 20].

To overcome the shortcomings of the above two models, many modified versions of the two-temperature model based on the high fidelity StS model or *ab initio* derived quasi-classical trajectory (QCT) rates have also been proposed. Mankodi and Myong [21] proposed two new models named the nonequilibrium total temperature (NETT) model and the nonequilibrium piecewise interpolation model. They claim that the new models are more accurate than Park's two-temperature model in simulating high-degree nonequilibrium flows [21]. Neitzel [18] develops two-temperature nonequilibrium, non-Boltzmann (2T-NENB) model. The 2T-NENB model is shown to reproduce the StS results well. In comparison to the non-Boltzmann direct molecular simulation (DMS) data, Chaudhry et al. [7, 22, 23] find that a simple correction can be applied to Marrone-Treanor (MT) model and achieve better agreement with non-Boltzmann data for dissociating flows. The modified MT model has been implemented in CFD solvers and used in simulating vehicle-scale hypersonic flows [22, 23].

The initial success of Chaudhry's non-Boltzmann correction model based on a limited number of numerical testings has demonstrated that it is a potentially effective way to improve the accuracy of the widely-used two-temperature models with a negligible increase in computational cost. However, this model has been applied only to the MT model, a semi-empirical one. Therefore, it is worth investigating its extensibility to other two-temperature models, including widely used empirical models and more sophisticated, physics-based models. Furthermore, more testings also need to justify the accuracy of widely-used and modified models, especially compared with available experimental measurements and high fidelity StS results.

The remainder of this paper is organized as follows. The governing equations for modeling hypersonic nonequilibrium flows are firstly presented in Sect. 2. After that, the widely-used and recent modification of two-temperature models is also introduced. Section 3 provides two typical cases to assess the performances of the original and modified version of two-temperature models. The discrepancies of results predicted by these models are also discussed and analyzed in Sect. 4. Conclusions are provided in Sect. 5.

2. Numerical methods

In this section, the governing equations for modeling hypersonic nonequilibrium flows are given first. We then present the most widely-used empirical two-temperature models and introduce the recent efforts to develop the correction method that enables these models to account for the effects of the non-Boltzmann vibrational energy distribution on chemical reactions.

2.1 Governing equation

Under the two-temperature assumptions, the governing equations for chemically reacting viscous flows are expressed as [24]

$$
\begin{cases}
\dfrac{\partial \rho_s}{\partial t}+\dfrac{\partial \rho_s u_j}{\partial x_j}=\dfrac{\partial}{\partial x_j}\left(\rho D_s \dfrac{\partial y_s}{\partial x_j}\right)+\omega_s, \\
\dfrac{\partial \rho u_i}{\partial t}+\dfrac{\partial \rho u_i u_j}{\partial x_j}=-\dfrac{\partial p}{\partial x_j}+\dfrac{\partial \tau_{ij}}{\partial x_j}, \\
\dfrac{\partial \rho E_v}{\partial t}+\dfrac{\partial \rho E_v u_j}{\partial x_j}=\dfrac{\partial}{\partial x_j}\left(\eta_v \dfrac{\partial T_v}{\partial x_j}\right)+\dfrac{\partial}{\partial x_j}\left(\rho \sum\limits_{s=1}^{ns} h_{v,s} D_s \dfrac{\partial y_s}{\partial x_j}\right)+\omega_v, \\
\dfrac{\partial \rho E}{\partial t}+\dfrac{\partial \rho H u_j}{\partial x_j}=\dfrac{\partial}{\partial x_j}\left(\eta_v \dfrac{\partial T_v}{\partial x_j}+\eta \dfrac{\partial T}{\partial x_j}\right) \\
\qquad\qquad +\dfrac{\partial}{\partial x_j}\left(\rho \sum\limits_{s=1}^{ns} h_s D_s \dfrac{\partial y_s}{\partial x_j}\right)+\dfrac{\partial \tau_{ij} u_i}{\partial x_j},
\end{cases}
\tag{1}
$$

where ρ is the density, u_j is the jth component velocity, ρ_s and y_s are the density and mass fraction of species s, E_v , E and H are the vibrational energy, total energy and total enthalpy per unit mass of mixture, D_s, η_v and η are the diffusion coefficient, thermal conductivity for vibrational energy and thermal conductivity for translational-rotational energy, $h_{v,s}$ and h_s are the vibrational and total enthalpy per unit mass of species s, τ_{ij} is the viscous stress tensor, p is pressure and calculated by Doltons law.

ω_s is the mass production rate of species s due to the chemical reactions and can be expressed as [24]

$$\omega_s = M_s \sum_{r=1}^{nr} (\beta_{rs} - \alpha_{rs}) \left[k_{f,r} \prod_{s=1}^{ns} \left(\frac{\rho_s}{M_s} \right)^{\alpha_{rs}} - k_{b,r} \prod_{s=1}^{ns} \left(\frac{\rho_s}{M_s} \right)^{\beta_{rs}} \right], \tag{2}$$

where nr and ns are the number of reactions and species, α_{rs} and β_{rs} are the stoichiometric coefficients for reactants and products in the r reaction respectively, $k_{f,r}$ and $k_{b,r}$ stand for the forward and backward rates for the r reaction respectively.

Furthermore, the source term of of vibrational energy ω_v is governed by [11]

$$\omega_v = \rho \frac{E_v(T) - E_v(T_v)}{\tau_v} + \omega_{vd}. \tag{3}$$

In Eq. (3), the first term on the right-hand side is the rate of translational-vibrational energy transfer according to Landau-Teller model [11]. τ_v is the vibrational relaxation time, which is usually evaluated by Millikan-White's formula. ω_{vd} is the vibrational energy change per dissociation [25], which is expressed as follows:

$$\omega_{vd} = E_b \omega_b - E_f \omega_f, \tag{4}$$

where ω_f and ω_b are destruction and production of diatoms due to dissociation, and E_f and E_b indicate the average vibrational energy lost and gained due to reactions.

The above equations are solved by an in-house code named advanced research tool in science and technology computational fluid dynamics (ARTIST-CFD), developed by the authors of State Key Laboratory of High-Temperature Gas Dynamics, Institute of Mechanics, Chinese Academy of Sciences. ARTIST-CFD is a parallel, finite volume code that solves two-dimensional, axisymmetric, and three-dimensional Navier-Stokes equations based on multi-block structured meshes. Roe upwind scheme with second-order MUSCL reconstruction and minmod limiter is applied for inviscid fluxes, and viscous fluxes are discretized by second-order central difference scheme [26, 27]. The data-parallel line relaxation (DPLR) scheme is employed for time marching [11]. A modified Fick's model is applied to calculate the species mass diffusion fluxes, ensuring that the sum of individual species' diffusion fluxes is zero [28]. The transport properties of mixture species are calculated according to Gupta's mixing rule [29], and the viscosity and thermal conductivity of species are calculated using collision cross-section data compiled by Scalabrin [11] and Wright et al. [30].

2.2 Two-temperature model

The semi-empirical Arrhenius equation is used to express the equilibrium forward reaction rates [11], and the backward rates are usually estimated based on the detailed balance theory [11]. In the framework of two-temperature model, the vibration-dissociation coupling effect, i.e., the effects of vibrational nonequilibrium on the dissociation rates, should be considered. Therefore, we can multiply the equilibrium reaction rate k_f by a nonequilibrium factor to give a nonequilibrium reaction rate k_f^{neq} [20, 25]:

$$k_f^{\text{neq}}(T, T_v) = Z(T, T_v) k_f(T), \tag{5}$$

where $Z(T, T_v)$ is the nonequilibrium factor. Note that k_f^{neq} is a function of both T and T_v while k_f is a function of only T.

Nowadays, many models considering the vibration-dissociation coupling effect have been proposed. In the following section, three semi-empirical or physics-based models are presented.

2.2.1 *Park model*

Compared the intensities of radiation emanating from the hot nitrogen and air behind a shock between measured and calculated, Park [31] proposed that the most appropriate control temperature in equilibrium reaction rates can be expressed as

$$T_a = T^{\alpha} T_v^{1-\alpha}, \tag{6}$$

where the value of α is usually chosen to be 0.5 or 0.7. In this study, $\alpha = 0.5$ is used and T_a is thus the geometric mean of T and T_v.

Therefore, the nonequilibrium factor of the Park model can be expressed as [20, 25]

$$Z(T, T_v) = \left(\frac{T_a}{T} \right)^n \exp\left(-\frac{\theta_d}{T_\alpha} + \frac{\theta_d}{T} \right), \tag{7}$$

where θ_d is the dissociation energy in K and n is the reaction parameters in the Arrhenius law.

The non-preferential model, which is widely-used with Park model, yields [11]

$$E_f = E_b = e_v, \tag{8}$$

which indicates that the loss of vibrational energy is the average vibrational energy e_v.

This model is straightforward to implement in a CFD code. However, it is a phenomenological model having many limitations in simulating hypersonic nonequilibrium flows [13]. Its applicability is only limited to the flow where vibrational distribution slightly deviates from equilibrium [13].

2.2.2 *MT model*

The MT model, also known as the coupled vibration-dissociation-vibration (CVDV) model, assumes that the vibrationally excited diatoms are more easily to dissociate [25,32]. The nonequilibrium factor of the MT model is given by [25,32]

$$Z(T,T_v)=\frac{Q(T)Q(T_F)}{Q(T_v)Q(-U)}, \tag{9}$$

where Q is the partition function for a truncated harmonic oscillator, U is the semi-empirical parameter and T_F is the temperature defined as [25,32]

$$T_F=\left(\frac{1}{T_v}-\frac{1}{T}-\frac{1}{U}\right)^{-1}. \tag{10}$$

The vibrational energy lost and gained with the MT model are expressed as [25]

$$\begin{cases} E_f=\dfrac{R_s\theta_v}{\exp\left(-\frac{\theta_v}{T_F}\right)-1}-\dfrac{R_s\theta_d}{\exp\left(-\frac{\theta_d}{T_F}\right)-1}, \\ E_b=\dfrac{R_s\theta_v}{\exp\left(-\frac{\theta_v}{U}\right)-1}-\dfrac{R_s\theta_d}{\exp\left(-\frac{\theta_d}{U}\right)-1}, \end{cases} \tag{11}$$

where θ_v is the species characteristic vibrational temperature, and R_s is the specific gas constant.

2.2.3 *Macheret-Fridman (MF) model*

The empirical two-temperature models cannot make reliable predictions when used outside the range of conditions (e.g., temperature) for calibrating them. Macheret et al. [33-35] and Adhikari et al. [36] developed a physics-based model for nonequilibrium dissociation reactions at high temperatures, known as the MF model. The MF model is derived based on the assumption of classical impulsive collision and has closed-form formulae. This model can well take the vibration-dissociation and rotation-dissociation couplings into account [35]. The dissociation reactions from the up-lying and low-lying vibrational states strongly depend on the vibrational and translational temperature, respectively.

The nonequilibrium factor of the MF model has the following form [35]:

$$Z(T,T_v)=\frac{1-\exp\left(-\frac{\theta_v}{T_v}\right)}{1-\exp\left(-\frac{\theta_v}{T}\right)}(1-L)\exp\left[-\theta_d\left(\frac{1}{T_v}-\frac{1}{T}\right)\right] + L\exp\left[-\theta_d\left(1-6a^2\right)\left(\frac{1}{T_a}-\frac{1}{T}\right)\right], \tag{12}$$

where L is a fractional parameter and T_a is a reduced temperature. T_a is expressed as [35]

$$T_a=aT_v+(1-a)T,\quad a=\left(\frac{m}{m+M}\right)^2, \tag{13}$$

in which m and M are the mass of atom in colliding particle and dissociating diatoms, respectively.

The fractional parameter L depends on the species involved in the collision. For diatom-atom collisions [35],

$$L=\frac{\sqrt{1-a}}{\pi^{3/2}}\sqrt{\frac{\theta_d}{D^*}}\left(\frac{T}{\theta_d}\right)^{1-n}\left[1+\frac{5(1-a)T}{2D^*}\right] \times\left[24\pi a(1-a)\frac{\theta_d}{T}\right]^{1/2}. \tag{14}$$

For diatom-diatom collisions [35],

$$L=\frac{2(1-a)}{\pi^2a^{3/4}}\left(\frac{\theta_d}{D^*}\right)\left(\frac{T}{\theta_d}\right)^{3/2-n}\left[1+\frac{7(1-a)(1+\sqrt{a})T}{2D^*}\right] \times\left[24\pi a(1-a)\frac{\theta_d}{T}\right]^{1/2}, \tag{15}$$

where D^* is the approximated value of effective dissociation energy, and can be expressed as

$$D^*=\theta_d-6a^2\theta_d. \tag{16}$$

The vibrational energy gained or lost for the MF model is [25]

$$E_f=E_b=\frac{aD^*(T_v/T_a)^2k_l+Dk_h}{k_l+k_h}, \tag{17}$$

where k_l and k_h are the dissociation rates for the low and high vibrational states, and formulated as [25]

$$\begin{cases} k_l=L\exp\left[-\theta_d\left(1-6a^2\right)\left(\dfrac{1}{T_a}-\dfrac{1}{T}\right)\right], \\ k_h=\dfrac{1-\exp\left(-\frac{\theta_v}{T_v}\right)}{1-\exp\left(-\frac{\theta_v}{T}\right)}(1-L)\exp\left[-\theta_d\left(\dfrac{1}{T_v}-\dfrac{1}{T}\right)\right]. \end{cases} \tag{18}$$

2.3 Improvement of two-temperature model

The widely-used two-temperature models can deal with the nonequilibrium between the vibrational and translational-rotational modes. However, the widely-used models assume that the energy in each mode is in a thermal equilibrium state and thereby follows the Boltzmann distribution. Some recent studies based on high-fidelity StS modeling reveal the existence of the non-Boltzmann distributions in dissociating flows [8, 9, 14, 17], indicating the importance of taking account of the non-Boltzmann effects in the simulations of highly thermal nonequilibrium flows.

2.3.1 *Modified MT model*

Chaudhry et al. [22, 23] compared the dissociate rate and the vibrational energy change per dissociation predicted by the MT model with those reproduced from the DMS for compression-type flows of N_2 and O_2. They found that there exist constant differences between the MT data and the DMS data. As DMS results show the vibrational energy distributions are non-Boltzmann, with high vibrational levels largely depleted, Chaudhry et al. [22] attributed the discrepancies between the MT-based and the DMS-based results to the non-Boltzmann effects and proposed the following non-Boltzmann correction models:

$$\begin{cases} k_f^{\mathrm{NB}} = \alpha_k^{\mathrm{NB}} k_f^{\mathrm{neq}}, \\ \omega_{vd}^{\mathrm{NB}} = \omega_{vd} + (\omega_f - \omega_b)\alpha_{\langle\epsilon\rangle}^{\mathrm{NB}} D_0, \end{cases} \tag{19}$$

where k_f^{NB} and $\omega_{vd}^{\mathrm{NB}}$ are the non-Boltzmann corrected dissociation rate and vibrational energy change per dissociation, respectively, D_0 is the dissociation energy of diatoms, k_f^{neq} and ω_{vd} are the nonequilibrium dissociation rate and vibrational energy change per dissociation in the widely-used two-temperature models, respectively.

Originally, Chaudhry et al. [23] adopted constant correction factors to set $\alpha_k^{\mathrm{NB}} = 0.5$ and $\alpha_{\langle\epsilon\rangle}^{\mathrm{NB}} = 0.1$. Very recently, Chaudhry et al. [22] proposed a variable non-Boltzmann (VNB) correction factor dependent on the chemical state. The VNB model was devised in such a way that α_k^{NB} approached 0.5 for rapidly dissociating flows 1.0 for chemical equilibrium flows in order to adapt to the DMS predictions [22]. Therefore, α_k^{NB} was finally determined to be

$$\alpha_k^{\mathrm{NB}} = \min\left\{\exp\left[\ln(0.5)\left(1 - \frac{[A][A]}{[A_2]k^{\mathrm{eq}}}\right)\right], 1\right\}. \tag{20}$$

The reaction rate parameters used in the MT model can be the same as those used in the widely-used two-temperature model based on the decades-old shock-tube data. Recently, developments in computational chemistry have encouraged the improvements of reaction rate coefficients. The QCT method, based on accurate *ab initio* potential energy surface (PES), has been employed to calculate reaction rate coefficients, and more accurate reaction rate parameters have been provided [21, 22]. Therefore, the dissociation rates of modified MT model are also calibrated by *ab initio* quantum chemistry data listed in Table 1 [22].

2.3.2 *Extension of the modified method*

Note that although Chaudhry et al. [22, 23] developed the non-Boltzmann correction method based on the MT model, the application of Eqs. (19) and (20) is independent of the specific two-temperature model in principle. Consequently, the general correction strategy outlined in this subsection can be combined with other commonly used two-temperature models, such as the empirical Park model and the physics-based model, to account for the vibrational non-Boltzmann effects.

Table 1 Quasi-classical trajectory derived rates [22]

A_2	M	$C\ \left(\mathrm{cm^3\ s^{-1}\ K^{-n}}\right)$	n	T_D (K)	θ_v (K)
N_2	N_2	5.9725×10^{-6}	–0.7017	117529	3411
N_2	N	1.3271×10^{-6}	–0.5625	113957	3411
N_2	O_2	8.3724×10^{-5}	–0.9991	116892	3415
O_2	O_2	6.1327×10^{-6}	–0.7695	60540	2280
O_2	O	1.5295×10^{-6}	–0.6541	60552	2280
O_2	N_2	3.0410×10^{-9}	–0.0223	59380	2263

The MF model is more physically rigorous and outperforms the empirical two-temperature models in a broader range of flow conditions, especially when the Arrhenius-type parameters are re-calibrated by the high-fidelity QCT data. However, it is still based on thermal equilibrium assumption within each internal mode. It thus cannot capture the effects of non-Boltzmann vibrational energy distributions on dissociation reactions. To enhance its capability of treating reacting flows with high thermal nonequilibrium degrees, we have extended the non-Boltzmann correction method discussed in Sect. 2.3.1 to be applied to the QCT calibrated MF model in this study. We refer to this new model as MMF.

3. Numerical experiments and validations

In this section, two typical cases (i.e., the postshock process of O_2 vibrational excitation and dissociation, and hypersonic flow past a sphere) are utilized to assess the performances of the modified models as well as the original two-temperature models. These models are carefully evaluated, and their results are compared in detail with the data of experiments and the high fidelity StS model.

3.1 Vibrational activation and dissociation in O_2 shock flows

Recently, vibrational temperature and mass fraction distributions of O_2 behind a normal shock wave are measured by Andrienko et al. [19] and Ibraguimova et al. [37]. Firstly, these experimental results are used to assess the performance of those aforementioned chemical kinetic models. The flow conditions for the test cases are tabulated in Table 2.

In the frame of reference moving with the shock wave, the governing equations for the flow can be simplified as stationary, inviscid one-dimensional Euler equation, and expressed as [8, 38]

Table 2 Flow conditions for post shock flow [19, 37]

Case	U_s (m/s)	P_∞ (Torr)	T_∞ (K)	Ma_∞
$C1$	3070	2.0	295	9.44
$C2$	3950	1.0	295	12.06
$C3$	4440	0.8	295	13.55

$$\frac{\partial}{\partial x}\begin{pmatrix}\rho_s u\\ \rho u^2+p\\ \rho u(h+u^2/2)\\ \rho u e_v\end{pmatrix}=\begin{pmatrix}\omega_s\\ 0\\ 0\\ \omega_v\end{pmatrix}, \tag{21}$$

where ω_s and ω_v are the chemical and vibrational energy source terms, respectively.

The above stiff equations are conducted from a shock wave reference frame and solved by a CVODE solver [39]. The initial conditions are derived from the Rankine-Hugoniot relations [8]. The simulations are performed on a uniform grid of 20000 nodes covering 2 cm in the distance behind the shock.

To validate the results predicted by the aforementioned two-temperature models, the StS simulation is also performed. For the StS approach, the vibrational energy equation in Eq. (21) is removed, and each vibrational energy level of oxygen is treated as pseudo-species. In the current study, 46 vibrational states of oxygen are considered [40]. The forced harmonic oscillator (FHO) model develops the kinetic rates of vibration-vibration-translation (V-V-T) bound-bound transitions for O_2-O_2 collision [9, 14]. The vibration-translation (V-T) rates for O_2-O collision and state-specific dissociation rates for O_2-O and O_2-O_2 collisions are obtained from Stellar database [40].

Figure 1a and b shows the profiles of vibrational temperature and mass fraction of O for the case $C1$, respectively. In the current study, Park, MT, and MF denote the original Park model [11], MT model [32], and MF model [35] employing Park 90 rates [11], respectively. Besides, MMT, MPark, and MMF represent the modified MT model proposed by

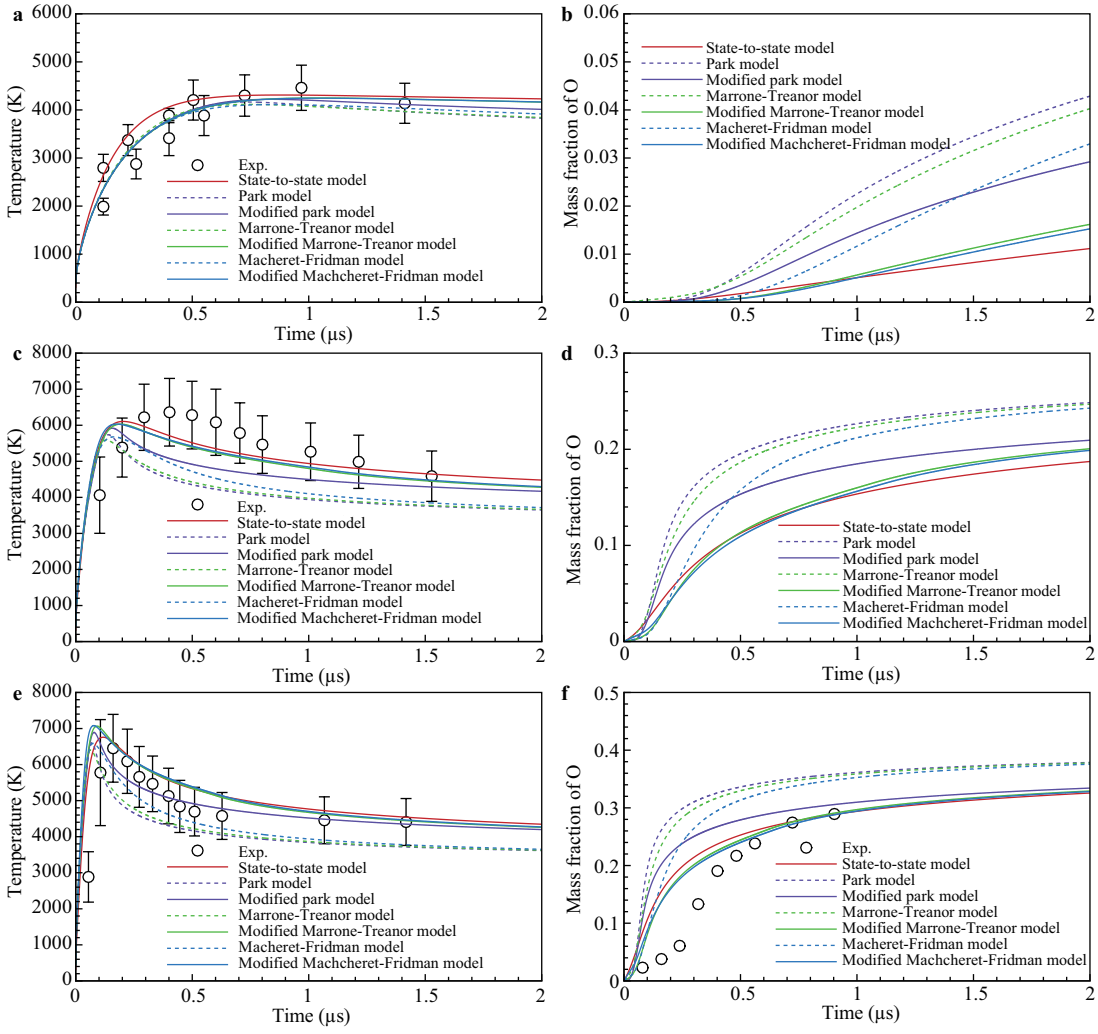

Figure 1 Profiles of vibrational temperature and mass fraction of O behind the shock. **a** Vibrational temperature for case $C1$, **b** mass fraction of O for case $C1$, **c** vibrational temperature for case $C2$, **d** mass fraction of O for case $C2$, **e** vibrational temperature for case $C3$, **f** mass fraction of O for case $C3$.

Chaudhry et al. [22, 23], the modified Park model, and the modified MF model proposed in this paper. Note that the corresponding rates of MPark, MMT, and MMF are replaced by the QCT fitted rates listed in Table 1. In this section, time is defined as the ratio of distance to shock velocity.

Figure 1a shows that all two-temperature models and the StS model predict similar tendencies in temperature profiles. Due to the mild post-shock temperature, a minimal amount of O_2 is dissociated. Figure 1b demonstrates that the mass fraction of O predicted by all two-temperature models at 2 μs is less than 4%. Therefore, vibration relaxation governed by O_2-O_2 collision is the major process in case $C1$. Due to the same vibrational relaxation time evaluated by Millikan-Whites formula used in Landau-Teller model [11], all the two-temperature models give similar temperature distributions that also show agreement with the experiments [19,37]. However, significant differences between the StS and two-temperature models can still be observed in the vibration relaxation and mass fraction of O. The thermal relaxation and dissociation rates predicted by the StS model are slightly faster and lower than the two-temperature model, respectively. Comparably, the mass fractions of O predicted by the MMF and MMT model are closer to the result of the StS model. The accuracy of the widely-used two-temperature model is acceptable in simulating weakly dissociation flows at mild temperatures.

For case $C2$, the profiles of vibrational temperature and mass fraction of O are plotted in Fig. 1c and d, respectively. Due to the higher shock velocity, a larger amount of O_2 dissociates after 0.1 μs which is nearly the ending time of vibrational relaxation. Park, MT, and MF models predict faster dissociation and lower vibrational temperature, which falls out of the error bar of experiment [19, 37]. Comparing the results of Park against the MPark model, the QCT derived parameters slow down the dissociation rate and increase the vibrational temperature, but the vibrational temperature predicted by MPark is still out of the error bar of experiment [19, 37]. By contrast, after 0.1 μs, the vibrational temperatures predicted by MMT and MMF model fall within the error bar of the experiment and agree well with the results of the StS model, implying that non-Boltzmann correction further reduces the dissociation rates. In addition, the mass fractions of O predicted by MMT and MMF model agree well with result of the StS model.

The vibrational temperature and mass fraction of O profiles for case $C3$ are shown in Fig. 1e and f, respectively. The case $C3$ represents the highest degree of nonequilibrium because of the highest shock velocity. The vibration relaxation terminates at nearly 0.1 μs, but dissociation occurs before the end of vibration relaxation. The vibrational temperatures predicted by these models show significant differences, but all the results are bounded by the large measurement uncertainties of vibrational temperatures [19,37]. However, it is illustrated that the vibrational temperature proposed by MMT and MMF model shows agreement with the result of the StS model. Furthermore, the mass fractions of O predicted by MMT and MMF model after 0.5 μs agree well with the experiments and result of the StS model. The widely-used two temperature models used Park 90 rates predict fast dissociation rate, and therefore, higher mass fraction of O behind the shock.

Figure 2 shows the variation of maximum vibrational temperature in terms of translational temperature measured after the shock. The maximum vibrational temperature predicted by the StS model is consistent with the experiments [19]. Generally, MPark, MMT, and MMF models accurately predict the maximum vibrational temperature. However, widely-used two-temperature models underestimate the maximum of vibrational temperature, especially under the condition of high translational temperature, i.e., high shock velocity.

3.2 Hypersonic flow past a sphere

Many numerical and experimental tests are performed to investigate the flow around a sphere, mimicking the extreme environments experienced by hypersonic vehicles [41, 42]. Recently, multi-dimensional StS computation for the five-species air mixture (N_2, O_2, NO, N, O) around a sphere is performed by Colonna et al. [42]. In their studies, 68 and 47 vibrational states are considered for N_2 and O_2 respectively, and only the ground state is considered for NO and atomic species. In total, an approximate amount of 10000 elementary processes are utilized, and the corresponding rates are calculated by SSH expression or QCT method [42]. Finally, detailed information on thermochemical nonequilibrium flow

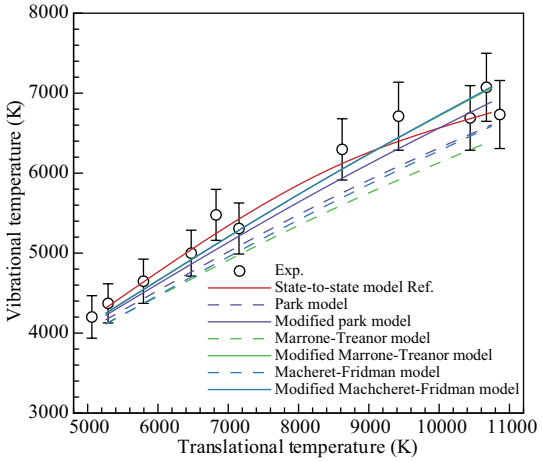

Figure 2 Maximum of vibrational temperature behind the shock.

and high fidelity results are provided [42]. Therefore, the flow past a sphere is also implemented to assess the performance of the aforementioned two-temperature models. The results are compared with the results of the StS model and experiments in detail.

ARTIST-CFD calculates the test cases in this section. Axisymmetric Navier-Stokes equations, including finite rate chemistry and the effects of thermal nonequilibrium, are solved based on multi-block structured meshes. The grid includes 120×200 cells and is refined near the shock wave. The freestream conditions are listed in Table 3. The freestream mass fractions of N_2 and O_2 are 0.767 and 0.233, respectively. In addition, the solid wall is modeled as non-catalytic (i.e., the gradients of species composition set to zero).

Figure 3a and b shows the Mach number profiles along the stagnation line for the cases $C4$ and $C5$, respectively, where the results of the two-temperature model, StS model, as well as shock location from experiments are shown for comparison. Figure 4a and b shows the mass fraction of O_2 and vibrational temperature profiles along the stagnation line for the case $C4$. Note that the StS model provides more accurate results, which agrees well with the experiments [42]. The original two-temperature models, including Park, MT, and MF models, obviously underestimate the shock stand-off distance (SSD). From the profiles of mass fraction of O_2 and vibrational temperature, we can find that the Park, MT, and MF models predict fast dissociation rates. Therefore, a lower vibrational temperature is predicted, which increases the density behind the shock and reduces the SSD. Compared with the results of the Park and MPark model, although QCT based rates significantly decrease the dissociation rates and predict thicker SSD, the SSD predicted by the MPark model is different from that of the StS model and still falls out of the error bar of experiment [42]. However, MMT and MMF models provide more accurate results, which show close agreement with the results of the StS model and nearly fall in the error bar of experiments [42].

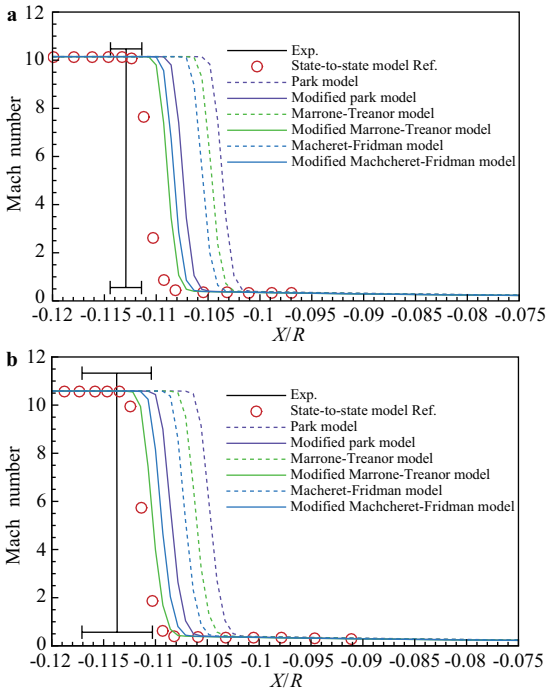

Figure 3 Mach number profiles at the shock position. **a** Case $C4$ and **b** case $C5$.

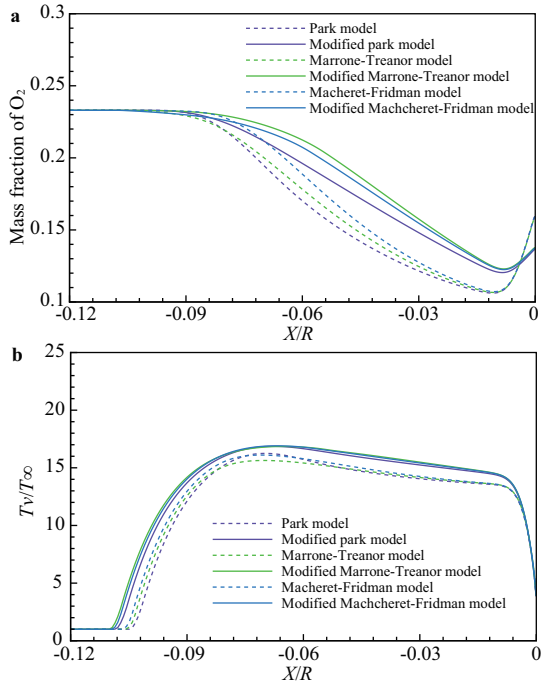

Figure 4 Mass fraction of O_2 and vibrational temperature profiles along the stagnation line for the case $C4$. **a** Mass fraction of O_2 and **b** vibrational temperature.

4. Analysis

In this section, two necessary inputs to CFD, dissociation rates and vibrational energy changes per dissociation of the aforementioned two-temperature models, are compared in detail. And the reason for improving the accuracy of modified two-temperature models is also analyzed and discussed. For the aforementioned case $C2$, a significant amount of O_2 is dissociated after the ending time of vibrational relaxation. Therefore, case $C2$ is selected as a typical sample for the dissociation-dominated flow in this section.

Table 3 Flow conditions for flow past a sphere [42]

Case	ρR (kg/m^2)	R (mm)	U_∞ (m/s)	T_∞ (K)	T_w (K)
$C4$	4×10^{-4}	7	3490	293	1000
$C5$	2×10^{-4}	7	3640	293	1000

4.1 The dissociation rate

To compare with the two-temperature result, the total dissociation rate from the StS model is defined as

$$k_f = \sum_{i=0}^{46} k_{f,i} \frac{[A_2(i)]}{[A_2]}, \tag{22}$$

where $k_{f,i}$ is the dissociation rate for vibrational state i.

Figures 5 and 6 show the total dissociation rate behind the shock for O_2-O_2 and O_2-O collisions respectively. The non-Boltzmann correction factor α_k^{NB} predicted by the MMT model is also plotted in Figs. 5 and 6. It is shown that the flow is near chemical equilibrium when the translational temperature goes down to 4800 K, i.e., $\alpha_k^{\mathrm{NB}} = 1$. The flow is in the state of chemical nonequilibrium when the translational temperature is higher than 4800 K.

Generally, the two-temperature models using Park90 rates predict the faster dissociation rates at lower translational temperature and underpredict it at higher translational temperature. Compared with the two-temperature models using Park-90 rates, modified models underestimate the dissociation rates. However, significant differences in dissociation rates still can be observed between modified models and the StS model. In the state of chemical nonequilibrium, the MMT and MMF model's dissociation rates are closer to that of the StS model. Previous studies show that O_2-O_2 collisions are the dominant process for case $C2$. Therefore, the agreement of dissociation rates of the StS and modified models is important for the improved vibrational temperature after the shock.

It is also shown that the MPark model predicts similar profiles with the Park model for O_2-O_2 collisions and underestimates the dissociation rates for O_2-O collisions. But, it may not be enough to get consistent results with the StS model. The compared study implies that the improvement of the widely-used Park two-temperature model is still limited even if the state-of-the-art QCT calibrated data is used. Some physics-based models, such as the MT and MF models, are more appropriate for the simulation of dissociation-dominated flow.

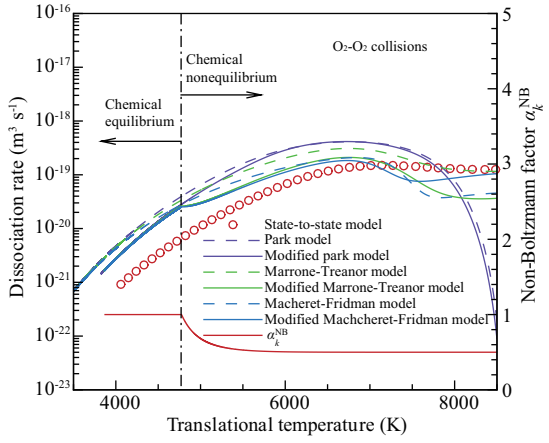

Figure 5 Dissociation rates for the O_2-O_2 collisions.

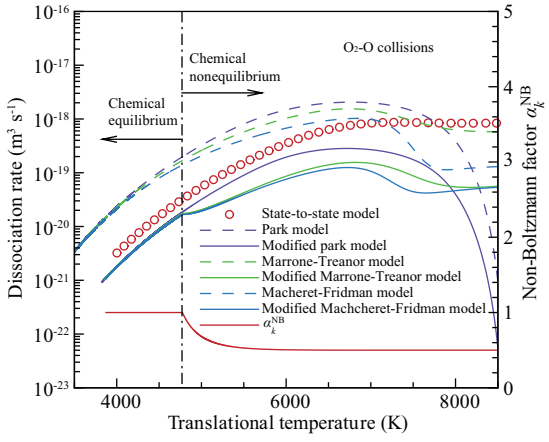

Figure 6 Dissociation rates for the O_2-O collisions.

Figure 5 shows that the dominant O_2-O_2 dissociation rates of the MMT and MF models are still two times faster than the StS model in the state of chemical equilibrium. Note that the MMT and MMF models' dissociation rates are closer to that of the StS model because $\alpha_k^{\mathrm{NB}} = 0.5$ multiplies the QCT refitted rates in the state of chemical nonequilibrium. We can probably infer that the QCT refitted dissociation rate of O_2-O_2 in Table 1 is two times faster. Therefore we reduce the dissociation rates by a factor of two and recalculate. In this section, only the results of MMF model are analyzed. The vibrational temperature and mass fraction of O profiles are shown in Fig. 7a and b, respectively. Under the condition of the same non-Boltzmann correction parameters used, reducing the dissociation rates by a factor of two significantly increases the vibrational temperature and reduces the mass fraction of O. However, only reducing the dissociation rates by a factor of two and without non-Boltzmann correction, i.e., $\alpha_k^{\mathrm{NB}} = 1$ everywhere, gets better results with the StS models.

On the whole, reducing the dissociation rates will slightly reduce the mass fraction of O. It is implied that if the equilibrium dissociation rates are refitted correctly, an improved agreement with the StS model can also be obtained even without considering the non-Boltzmann correction. However, it needs to be further investigated because the modification of the MMT model is proposed on the adiabatic heat bath simulation whose temperature is much higher than case $C2$ [43]. Machine learning may offer techniques to extract information from large amounts of QCT and high fidelity StS data that can be used for the improvement of widely-used two temperature model [44].

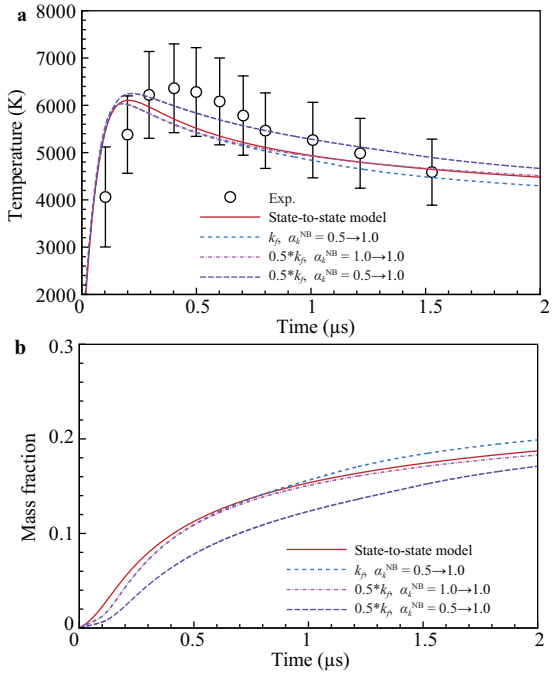

Figure 7 Effect of dissociation rates on the vibrational temperature and mass fraction of O. **a** Vibrational temperature and **b** mass fraction of O.

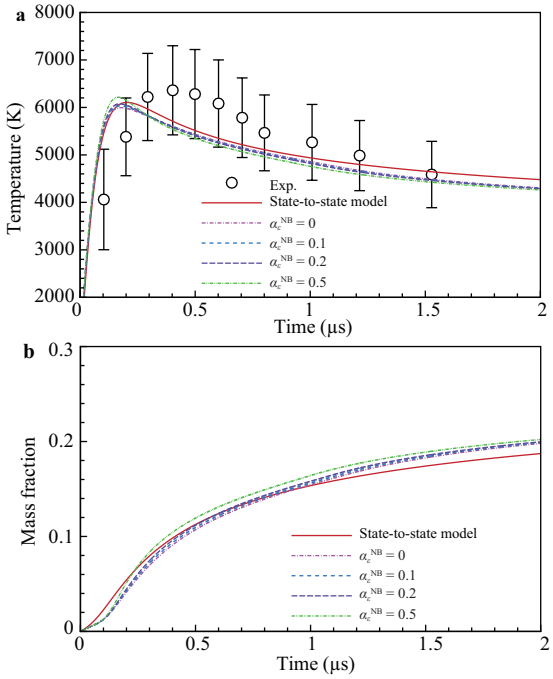

Figure 8 Effect of non-Boltzmann corrected parameter $\alpha_{\langle\epsilon\rangle}^{NB}$ on the vibrational temperature and mass fraction of O. **a** Vibrational temperature and **b** mass fraction of O.

4.2 The vibrational energy change per dissociation

By comparing the results of the MT model and DMS method for adiabatic heat bath, Chaudhry et al. [23] find that the vibrational energy loss per dissociation of MT model is nearly 10% higher than DMS method. Therefore $\alpha_{\langle\epsilon\rangle}^{NB} = 0.1$ is used in MMT model to reduce dissociation energy of O_2 [23]. Nonetheless, Baluckram and Andrienko [43] note that the MMT model still overestimates the vibrational energy loss per dissociation. Therefore, we increase the $\alpha_{\langle\epsilon\rangle}^{NB}$ and investigate the effect on the vibrational temperature and mass fraction of O. The results are shown in Fig. 8a and b. The maximum vibrational temperature post the shock increases with increasing $\alpha_{\langle\epsilon\rangle}^{NB}$ that decreases the vibrational energy loss. In general, changing the value of $\alpha_{\langle\epsilon\rangle}^{NB}$ from 0 to 0.5 does not significantly affect the vibrational temperature and mass fraction of O. It is also indicated that the accuracy of vibrational energy loss per dissociation of the MT model is acceptable, i.e., $\alpha_{\langle\epsilon\rangle}^{NB} = 0$. Comparatively, modifying dissociation rates has more influence on the distribution of vibrational temperature and mass fraction of O than changing the value of $\alpha_{\langle\epsilon\rangle}^{NB}$.

5. Conclusions

The correction method of the modified MT model is successfully applied and extended to the physics-based MF model. After that, the performance and accuracy of the modified and widely-used two-temperature models are assessed in detail by two typical tests.

The numerical results show that the widely-used two-temperature model fails to predict the highly nonequilibrium dissociating flows. Compared with the Park 90 rates used in widely-used two-temperature models, the QCT data utilized in modified models indicate slower dissociation rates. In addition, the non-Boltzmann effect further reduces the dissociation rates and vibrational energy per dissociation. Consequently, the dissociation rates predicted by modified models are closer to the rates of the StS model. Therefore, better agreements with the StS modeling and experiments are provided.

However, a significant difference in dissociation rates still can be observed between modified models and the high fidelity StS model. Comparatively, equilibrium dissociation rates have more influence on the distribution of vibrational temperature and mass fraction of O than changing the value of non-Boltzmann factor for vibrational energy loss per dissociation. Suppose the equilibrium dissociation rates are refitted correctly, and more physical-based vibrational-dissociation coupling models are used. In that case, an improved agreement with the StS model can also be obtained without considering the non-Boltzmann correction.

On the whole, this work indicates that the correction method based on the MT model is easily applied and extended to the other widely-used two-temperature model. The modified form is promising for further development to design the high fidelity and effective kinetic model for engineering applications.

Author contributions *Xiaoyong Wang and Qizhen Hong designed the research and wrote the first draft of the manuscript. Yuan Hu and Qunhua Sun helped organize the manuscript, revised and edited the final version.*

Acknowledgements *This work was supported by the National Key Research and Development Program of China (Grant No. 2019YFB1704204) and the National Natural Science Foundation of China (Grant No. 12002348). The authors thank Dr. Jiaao Hao at the Hong Kong Polytechnic University for providing the O_2-O_2 V-V-T transition rate coefficients.*

1 G. Tu, J. Chen, X. Yuan, Q. Yang, M. Duan, Q. Yang, Y. Duan, X. Chen, B. Wan, and X. Xiang, Progress in flight tests of hypersonic boundary layer transition, Acta Mech. Sin. **37**, 1589 (2021).
2 G. V. Candler, Rate-dependent energetic processes in hypersonic flows, Prog. Aerospace Sci. **72**, 37 (2015).
3 P. A. Gnoffo, Planetary-entry gas dynamics, Annu. Rev. Fluid Mech. **31**, 459 (1999).
4 G. V. Candler, Rate effects in hypersonic flows, Annu. Rev. Fluid Mech. **51**, 379 (2019).
5 Y. Ye, How does the rarefaction of the air affect hypersonic vehicles, Acta Mech. Sin. **37**, 18 (2021).
6 D. Peng, X. Liu, L. Jiao, Z. Li, X. Wen, C. Yuan, G. Han, Y. Liu, Y. Liu, and Z. Jiang, Noise reduction for temperature-sensitive paint measurement contaminated by strong background radiation in a high enthalpy hypersonic tunnel, Acta Mech. Sin. **37**, 20 (2021).
7 R. S. Chaudhry, Modeling and Analysis of Chemical Kinetics for Hypersonic Flows in Air, Dissertation for Doctoral Degree (The University of Minnesota, Twin Cities, 2018).
8 K. Neitzel, D. Andrienko, and I. D. Boyd, Aerothermochemical nonequilibrium modeling for oxygen flows, J. Thermophys. Heat Transfer **31**, 634 (2017).
9 Q. Hong, X. Wang, Y. Hu, and Q. Sun, Development of a stagnation streamline model for thermochemical nonequilibrium flow, Phys. Fluids **32**, 046102 (2020).
10 D. Hash, J. Olejniczak, M. Wright, D. Prabhu, M. Pulsonetti, B. Hollis, P. Gnoffo, M. Barnhardt, I. Nompelis, and G. Candler, in FIRE II calculations for hypersonic nonequilibrium aerothermodynamics code verification: DPLR, LAURA, and US3D: Proceedings of 45th AIAA Aerospace Sciences Meeting and Exhibit, Reno, 2007.
11 L. C. Scalabrin, Numerical Simulation of Weakly Ionized Hypersonic Flow over Reentry Capsules, Dissertation for Doctoral Degree (The University of Michigan, Ann Arbor, 2007).
12 I. Nompelis, and G. V. Candler, in US3D predictions of double-cone and hollow cylinder-flare flows at high-enthalpy: Proceedings of 44th AIAA Fluid Dynamics Conference, Atlanta, 2014.
13 G. V. Candler, P. K. Subbareddy, and J. M. Brock, Advances in computational fluid dynamics methods for hypersonic flows, J. Spacecraft Rockets **52**, 17 (2015).
14 J. Hao, J. Wang, and C. Lee, State-specific simulation of oxygen vibrational excitation and dissociation behind a normal shock, Chem. Phys. Lett. **681**, 69 (2017).
15 A. Munafó, Y. Liu, and M. Panesi, Modeling of dissociation and energy transfer in shock-heated nitrogen flows, Phys. Fluids **27**, 127101 (2015).
16 L. Campoli, O. Kunova, E. Kustova, and M. Melnik, Models validation and code profiling in state-to-state simulations of shock heated air flows, Acta Astronaut. **175**, 493 (2020).
17 D. A. Andrienko, and I. D. Boyd, High fidelity modeling of thermal relaxation and dissociation of oxygen, Phys. Fluids **27**, 116101 (2015).
18 K. J. Neitzel, Thermochemical Modeling of Nonequilibriumoxygen Flows, Dissertation for Doctoral Degree (The University of Michigan, Ann Arbor, 2017).
19 D. Andrienko, and I. D. Boyd, in Vibrational relaxation and dissociation in O_2-O mixtures: Proceedings of 46th AIAA Thermophysics Conference (American Institute of Aeronautics and Astronautics, Reston, 2016).
20 Q. Hong, X. Wang, and Q. Sun, Detailed analysis of vibrational states of oxygen in high temperature non-equilibrium flows, Chin. J. Theor. Appl. Mech. **51**, 1761 (2019).
21 T. K. Mankodi, and R. S. Myong, Quasi-classical trajectory-based non-equilibrium chemical reaction models for hypersonic air flows, Phys. Fluids **31**, 106102 (2019).
22 R. S. Chaudhry, I. D. Boyd, and G. V. Candler, in Vehicle-scale simulations of hypersonic flows using the MMT chemical kinetics model: Proceedings of AIAA Aviation 2020 Forum (American Institute of Aeronautics and Astronautics, Reston, 2020).
23 R. S. Chaudhry, I. D. Boyd, E. Torres, T. E. Schwartzentruber, and G. V. Candler, in Implementation of a chemical kinetics model for hypersonic flows in air for high-performance CFD: Proceedings of AIAA Scitech 2020 Forum, Orlando (American Institute of Aeronautics and Astronautics, Reston, 2020).
24 X. Y. Wang, C. Yan, Y. K. Zheng, and E. L. Li, Assessment of chemical kinetic models on hypersonic flow heat transfer, Int. J. Heat Mass Transfer **111**, 356 (2017).
25 M. Panesi, Physical Models for Nonequilibriumplasma Flow Simulations at Highspeed Re-entry Conditions, Dissertation for Doctoral Degree (Universita degli Studi di Pisa, Pisa, 2009).
26 X. Wang, Numerical Research on Hypersonic Thermo-Chemical-nonequilibrium and Equilibrium Flows, Dissertation for Doctoral Degree (Beihang University, Beijing, 2018).
27 K. Zhong, Influence of Key Factors of High Temperature Gas Effect and its Mechanism Analysis, Dissertation for Doctoral Degree (Beihang University, Beijing, 2020).
28 H. Alkandry, I. D. Boyd, and A. Martin, Comparison of transport properties models for flowfield simulations of ablative heat shields, J. Thermophys. Heat Transfer **28**, 569 (2014).
29 R. N. Gupta, J. M. Yos, R. A. Thompson, and K. P. Lee, A Review of Reaction Rates and Thermodynamic and Transport Properties for an 11-species Air Model for Chemical and Thermal Nonequilibrium Calculations to 30000 K, Technical Report, 1990.
30 M. J. Wright, D. Bose, G. E. Palmer, and E. Levin, Recommended collision integrals for transport property computations, Part 1: Air species, AIAA J. **43**, 2558 (2005).
31 C. Park, Nonequilibrium Hypersonic Aerothermodynamics (Wiley-Interscience, New York, 1990).
32 P. V. Marrone, and C. E. Treanor, Chemical Relaxation with preferential dissociation from excited vibrational levels, Phys. Fluids **6**, 1215 (1963).
33 S. O. Macheret, and J. W. Rich, Nonequilibrium dissociation rates behind strong shock waves: Classical model, Chem. Phys. **174**, 25 (1993).
34 S. O. Macheret, A. A. Fridman, I. V. Adamovich, J. W. Rich, and C. E. Treanor, in Mechanisms of nonequilibrium dissociation of diatomic molecules: Proceedings of 6th Joint Thermophysics and Heat Transfer Conference, Colorado Springs, 1994.
35 H. Luo, A. A. Alexeenko, and S. O. Macheret, Assessment of classical impulsive models of dissociation in thermochemical nonequilibrium, J. Thermophys. Heat Transfer **32**, 861 (2018).
36 N. Adhikari, and A. A. Alexeenko, A general form of Macheret-Fridman classical impulsive dissociation model for nonequilibrium flows, Phys. Fluids **33**, 056109 (2021).
37 L. B. Ibraguimova, A. L. Sergievskaya, V. Y. Levashov, O. P. Shatalov, Y. V. Tunik, and I. E. Zabelinskii, Investigation of oxygen dissociation and vibrational relaxation at temperatures 4000-10800 K, J. Chem. Phys. **139**, 034317 (2013).
38 W. Su, D. Bruno, and Y. Babou, State-specific modeling of vibrational relaxation and nitric oxide formation in shock-heated air, J. Thermophys. Heat Transfer **32**, 337 (2018).
39 S. D. Cohen, A. C. Hindmarsh, and P. F. Dubois, CVODE, A stiff/nonstiff ODE solver in C, Comput. Phys. **10**, 138 (1996).
40 M. Lino da Silva, B. Lopez, V. Guerra, and J. Loureiro, A multiquantum state-to-state model for the fundamental states of air: The stellar

database, ESA Spec. Publ. **714**, 16 (2012).
41 S. Nonaka, H. Mizuno, K. Takayama, and C. Park, Measurement of shock standoff distance for sphere in ballistic range, J. Thermophys. Heat Transfer **14**, 225 (2000).
42 G. Colonna, F. Bonelli, and G. Pascazio, Impact of fundamental molecular kinetics on macroscopic properties of high-enthalpy flows: The case of hypersonic atmospheric entry, Phys. Rev. Fluids **4**, 1 (2019).
43 V. T. Baluckram, and D. Andrienko, in First-principle simulation of vibrational activation and dissociation in oxygen shock flows: Proceedings of AIAA Scitech 2021 Forum (American Institute of Aeronautics and Astronautics, Reston, 2021).
44 S. L. Brunton, B. R. Noack, and P. Koumoutsakos, Machine learning for fluid mechanics, Annu. Rev. Fluid Mech. **52**, 477 (2020), arXiv: 1905.11075.

高超声速热化学非平衡流动双温度模型的精度研究

王小永, 洪启臻, 胡远, 孙泉华

摘要 由于一些经验性的假设, 高超声速热化学非平衡流动模拟中广泛使用的双温度模型包含很大的不确定性. 为了克服传统双温度模型的缺陷, 本文基于修正Marrone-Treanor model的方法建立了修正的Macheret-Fridman model. 一些典型的算例被用来验证上述修正模型和广泛采用的双温度模型的精度. 此外, 本文重点分析和讨论了修正模型预测精度提高的原因. 研究结果表明, 基于Marrone-Treanor model的修正方法可以推广至传统的双温度模型中, 并显著提高其预测精度. 此外, 精确模拟高超声速热化学非平衡流动需要考虑三个方面的因素: 离解速率、振动-离解耦合作用以及非Boltzmann效应. 非Boltzmann效应降低了离解速率和振动导致的离解能变化. 对比而言, 离解速率的影响大于非Boltzmann效应导致的离解能的变化. 为了提高传统双温度模型的预测精度, 未来工作可以主要集中在提高离解速率的精度上面.